Journal of Cell Communication and Signaling (2019) 13:129–143
https://doi.org/10.1007/s12079-018-0498-7

NUTS AND BOLTS

A reproducible scaffold-free 3D organoid model to study neoplastic progression in breast cancer

Sabra I. Djomehri[1,2,3] · Boris Burman[1] · Maria E. Gonzalez[1] · Shuichi Takayama[4,5] · Celina G. Kleer[1,3]

Received: 17 October 2018 / Accepted: 21 November 2018 / Published online: 4 December 2018

Abstract

While 3D cellular models are useful to study biological processes, gel-embedded organoids have large variability. This paper describes high-yield production of large (~1 mm diameter), scaffold-free, highly-spherical organoids in a one drop-one organoid format using MCF10A cells, a non-tumorigenic breast cell line. These organoids display a hollow lumen and secondary acini, and express mammary gland-specific and progenitor markers, resembling normal human breast acini. When subjected to treatment with TGF-β, the hypoxia-mimetic reagent $CoCl_2$, or co-culture with mesenchymal stem/stromal cells (MSC), the organoids increase collagen I production and undergo large phenotypic and morphological changes of neoplastic progression, which were reproducible and quantifiable. Advantages of this scaffold-free, 3D breast organoid model include high consistency and reproducibility, ability to measure cellular collagen I production without noise from exogenous collagen, and capacity to subject the organoid to various stimuli from the microenvironment and exogenous treatments with precise timing without concern of matrix binding. Using this system, we generated organoids from primary metaplastic mammary carcinomas of MMTV-Cre;*Ccn6*$^{fl/fl}$ mice, which retained the high grade spindle cell morphology of the primary tumors. The platform is envisioned to be useful as a standardized 3D cellular model to study how microenvironmental factors influence breast tumorigenesis, and to potential therapeutics.

Keywords 3D cell culture · Organoids · Hanging drop · Human breast cancer · Morphogenesis · Phenotype · Microenvironment · EMT · Mesenchymal stromal cells · Metaplastic · CCN6

Shuichi Takayama and Celina G. Kleer contributed equally to this work.

Electronic supplementary material The online version of this article (https://doi.org/10.1007/s12079-018-0498-7) contains supplementary material, which is available to authorized users.

✉ Shuichi Takayama
takayama@gatech.edu

✉ Celina G. Kleer
kleer@umich.edu

[1] Department of Pathology, University of Michigan Medical School, Ann Arbor, MI 48109, USA

[2] Molecular and Cellular Pathology Training Program, University of Michigan, Ann Arbor, MI 48109, USA

[3] Rogel Cancer Center, University of Michigan, Ann Arbor, MI 48109, USA

[4] Department of Biomedical Engineering, Biointerfaces Institute, University of Michigan, Ann Arbor, MI, USA

[5] Wallace H. Coulter Department of Biomedical Engineering, Georgia Institute of Technology, Atlanta, GA, USA

Introduction

The use of three-dimensional (3D) cell culture models has increased the understanding of breast cancer progression, enabled testing of new treatments, and may offer a unique platform for high throughput analyses of molecular changes during breast initiation, progression, and metastasis. However, there is a need for novel models that better recapitulate the mammary gland architecture while also offering reproducible quantitative parameters.

Being more physiologically relevant than conventional two-dimensional (2D) culture, cells grown in 3D are capable of organizing into distinct phenotypes resembling miniature functional units of the breast. Early investigations using a laminin-rich matrix, commonly known as Matrigel (Barcellos-Hoff et al. 1989; Petersen et al. 1992), or a collagen matrix (Simian et al. 2001), demonstrated that mammary morphogenesis, mammary gland branching, and discernment of normal and neoplastic mammary phenotypes are assayable domains. Notable follow-up studies laid the framework for standard 3D culture procedures for breast

models existing today (Debnath et al. 2003; Lee et al. 2007). In 3D culture, non-tumorigenic MCF10A cells form 3D microstructures called acini, which are generated either by embedding cells inside or on top of Matrigel. These scaffold-based systems have particular advantages when studying early events of tumor initiation, cell-extracellular matrix (ECM) biophysical interactions (Chandler et al. 2011; Venugopalan et al. 2014), and tumor migration and invasion (Vinci et al. 2012; Pal and Kleer 2014; Pal et al. 2012). However, although these systems mimic facets of the in vivo microenvironment, the ECM scaffold can adsorb and trap growth factors, cytokines, and chemokines, and may not be ideal to test treatment effects.

Liquid-based systems, on the other hand, like the hanging drop technique, allow for media exchanges and administration of chemical components with flexible timing. Others have achieved spheroid reproducibility using 96-well hanging drop systems (Vinci et al. 2012; Thoma et al. 2013) and even automated hanging drop culture with digital microfluidics (Aijian and Garrell 2015) to generate a single spheroid per well. We have also developed a high-throughput 384-well hanging drop platform (Tung et al. 2011) that simplified the conventional hanging drop method, including optimized media additives (Leung et al. 2015). The macromolecular additive methylcellulose (MethoCel) and a low concentration of Matrigel to the culture media only upon cell seeding contributed to highly uniform, compact spheroid morphologies. This system has allowed the development of spheroids from breast cancer cells (Leung et al. 2015), but until now has not been well explored using non-tumorigenic mammary epithelial cells to achieve consistent 3D structures, which demonstrate the challenges of slow or inefficient reaggregation capacity in a liquid-based setting (Nakano et al. 2012).

Recent advances in cell culture are steering research towards organotypic culture (Fig. 1a). Organotypic culture is characterized by the physiologic interaction of multiple cellular phenotypes to recapitulate the fundamental unit of the tissue of origin, the resulting cellular constructs often referred to as "organoids," whereas "spheroids" loosely describe 3D structures or cellular aggregates that may self-organize but need not recapitulate a tissue-like behavior (diagram, Fig. 1b). Here, we define an "organoid," similar to that described in a recent review (Marina and Bissell 2017), as a 3D structure that self-organizes in culture to reproduce the basic functional unit of the native tissue.

In this study we use a scaffold-free 384-well hanging drop system to culture non-tumorigenic mammary MCF10A cells, MDA-MB-231 breast cancer cells, and primary carcinomas of MMTV-Cre;*Ccn6*$^{fl/fl}$ mice. We show that MCF10A cells are able to expand into organoids that resemble the architecture of normal human breast including presence of multiple cellular phenotypes (Debnath et al. 2003). We found that laminin-rich components and not a laminin-rich matrix, together with a simple crowding agent and FBS in 3D suspension culture is sufficient to support formation of mammary acinar structures of high reproducibility, and that using scaffold free-culture, MCF10A cells form a large, self-organized mammary gland (MG)-like organoid structure capable of exhibiting multiple lineage phenotypes. We demonstrate the ability to generate organoids from primary metaplastic carcinomas of MMTV-Cre;*Ccn6*$^{fl/fl}$ mice that contain tumor cells and cells from the microenvironment. Importantly, we provide a new physiologically relevant 3D organoid model, able to recapitulate normal breast and neoplastic progression.

Results & discussion

Establishment and expansion of a scaffold-free 3D MCF10A breast organoid model

Modeling neoplastic progression in mammary organoids with multiple phenotypes and mixed cell populations remains a challenge (Gusterson et al. 2005). A classic work by Wellings and colleagues (Wellings 1980) further supported by recent studies investigating cell-of-origin of breast cancers, suggests that human breast cancers originate from cells within the terminal duct lobular unit (TDLU, Fig. 1a), a composite of a duct and several lobules. In this study, we have generated a 3D mammary gland-like structure with similarities signature and structural aspects of the normal breast.

In a previous report from our group (Leung et al. 2015), we found improved spheroid formation in a 384-well hanging drop system on spheroids derived from cancer cell lines using both Matrigel, collagen and other ECM hydrogel scaffolds. However, MCF10A cells were unable to aggregate into tight single structures under these conditions (Fig. 2a no FBS conditions). Here, we demonstrate that under specific conditions, MCF10A cells form tight compact aggregates. Further, we show that the scaffold-free environment allows 3D MCF10A organoids with hollow lumen to expand up to diameters of 1.2 mm as well as display multiple lineage markers (Fig. 1a, top panel). The large 3D organoids may also contain one or more acini (Fig. 1a, bottom panel, acini indicated by white arrows). Because these features are distinct from previous reports of MCF10A acini (Debnath et al. 2003; Pal and Kleer 2014; Pal et al. 2012; Vidi et al. 2013), and produce multiple cell lineages as should be observed in organotypic cultures (Yin et al. 2016), we refer to these 3D structures as MCF10A organoids.

Typically, MCF10A acini in the literature including studies from our lab (Lee et al. 2007; Pal and Kleer 2014; Pal et al. 2012), have matched physiologic acinar sizes (50–200 μm), but the MCF10A organoids formed here in hanging drop ranged from 900 to 1200 μm and 1070 ± 105 μm average diameter after 2 weeks in culture and typically exhibited multi-acinar structures resembling aspects of normal breast TDLU. These differences are depicted in Fig. 1b, which shows conventional MCF10A scaffold-based culture with polarized acini embedded in Matrigel (leftmost) or conventional spheroids grown in U-

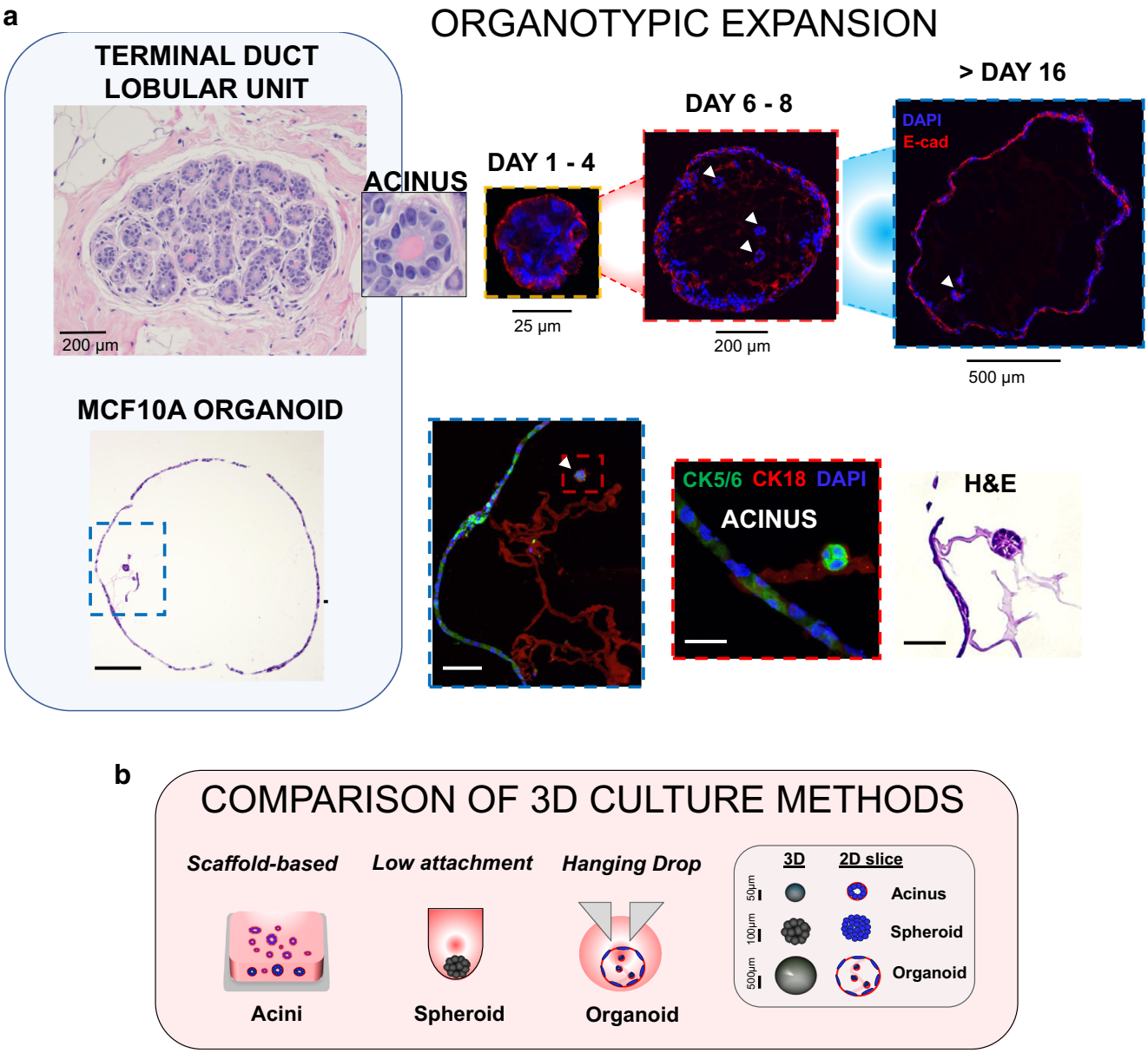

Fig. 1 Organotypic expansion in MCF10A cells cultured in 3D hanging drop system. a TOP PANEL: representative image of a normal terminal duct lobular unit (TDLU) in a human breast tissue sample (University of Michigan IRB HUM00050330) and inset showing an acinar structure comparing with organoid formation through 16 days, with expression of epithelial marker E-cadherin and hollow lumen formation. White arrows indicate 3D acinar structures within organoids. BOTTOM PANEL: 3D MCF10A organoid after 16 days by H&E showing a large hollow structure (scale bar = 200 µm), blue inset at 20X showing internal features (scale bar = 50 µm), red inset at 60X magnification of a developing acinar structure (scale bar = 15 µm) (confocal images: CK5/6 = green, CK18 = red, nuclei = DAPI) and corresponding H&E image (scale bar = 15 µm). **b** diagram of conventional scaffold-based Matrigel culture or U-bottom spheroid formation compared with the hanging drop system. Legend shows characteristic sizes of acini, spheroid or organoid structures grown in 3D

bottom plates (middle), MCF10A organoids developed in this study (rightmost), and legend showing typical sizes of the different biological structures formed in 3D. The size of the organoids may reflect not only the tightness of cellular interactions within the organoid but may also be a critical determinant of cell biology (Thoma et al. 2014). As seen in recent organotypic culture studies, larger sphere sizes may correlate with the ability of organoids to generate and display multiple phenotypes in 3D, as with multilayered optic cup structures from hESCs of ~550 µm diameters (Nakano et al. 2012), to human brain organoids of ~2 mm diameters that produced regions of multiple cell types (Quadrato et al. 2017). Furthermore, Cerchiari and colleagues found that robust self-organization and controllability of mammary epithelial cells in 3D is governed by properties of the surrounding medium, and

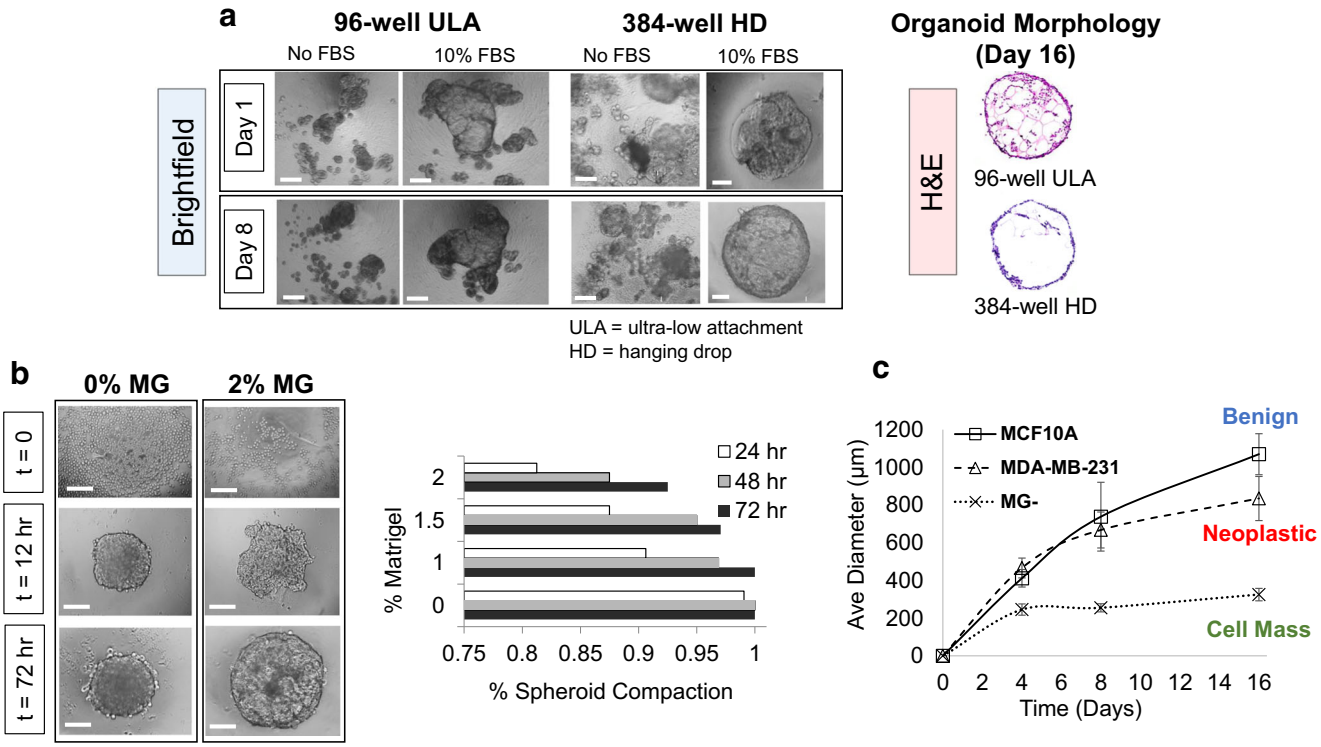

Fig. 2 Optimization of organoid formation technique in 384-well hanging drop (HD) system. a Representative brightfield images of 96-well ultra-low attachment (ULA) or 384-well HD 3D culture methods without FBS and with 10% FBS at days 1 and 8, and corresponding H&E sections at day 16. **b** 0% and 2% Matrigel (*v*/v) at $t = 0$, 12, and 72 h (scalebar = 100 μm), and measurements of spheroid compaction efficiency rate at 0%, 1%, 1.5% and 2% Matrigel (v/v) at 24, 48 and 72 h ($N = 25$ per subgroup). **c** average diameter of benign, neoplastic, and cell mass organoid subgroups (MCF10A, MDA-MB-231, and 0% Matrigel (MG^-), respectively) and time-course measurements at t = 0 through day 16. Average diameter was measured by morphometric analyses in triplicate using $N = 10$ organoids per subgroup, where best fit ellipsoids of round or irregular organoid morphologies were determined using Feret's statistical diameter in ImageJ. Scalebar = 500 μm for 96-well ULA and 150 μm for 384-well HD brightfield images

need not be a traditional ECM scaffold (Cerchiari et al. 2015). This might explain the high controllability we observe in MCF10A organoids, in which the cell-droplet boundary may promote better self-organizing properties.

More critically, the use of MCF10A as a suitable cell line to model normal breast cell function has been established in the field (Petersen et al. 1992; Debnath et al. 2003; Gaiko-Shcherbak et al. 2015). More recently, Qu and others (Qu et al. 2015) found a mixed luminal and basal expression was observed. Our results confirm mixed luminal and basal expression of MCF10A organoids. As shown in Fig. 1, MCF10A organoids expressed the basal marker cytokeratin (CK) 5/6 on the basolateral side, and luminal markers CK 18 and E-cadherin on the apical side facing the lumen. Cytokeratin status has been intensely studied in clinical pathology on breast lesions and benign tissue, with distinct phenotypes described as stem/progenitor (CK 5/6+), glandular progenitor (CK 5/6+ and CK 18+), and committed glandular (CK 18+) (Boecker and Buerger 2003; Abd El-Rehim et al. 2004). Interestingly, a population of CK 5/6+ cells on the basolateral side of MCF10A organoids appeared to co-express CK 18, suggesting glandular progenitor status. Supporting these data, recent studies generating TDLU-like organoids from primary human mammary epithelial cells found that the TDLU signature consisted of a co-expression of multiple lineage makers at similar positions as we observed in MCF10A organoids and in normal human TLDU (Gusterson et al. 2005; Linnemann et al. 2015). Together, these results support that the MCF10A model, when grown into 3D organoids, recapitulates features of the cellular heterogeneity of the normal breast TDLU.

Growth and remodeling of normal mammary organoids

The ability to form physiologic acinar structures in 3D is generally thought to require a scaffold-based setting because the support matrix provides the necessary pseudo-basement membrane. However, based on our studies, we postulate that the scaffold material itself might limit organoid expansion, by mechanical constraints and/or limiting the supply of critical nutrients (Lesher-Pérez et al. 2017), thus, MCF10A 3D structures only develop into smaller acinar structures of singular phenotype.

Since non-tumorigenic MCF10A cells are known to form acini in 3D without stemness capacity (Qu et al. 2015), we predicted low expansion ability in hanging drop. However, we found that a combination of low Matrigel concentration (~1–2%) and higher serum (10% FBS) at seeding strikingly promoted expansion of organoids (Fig. 2a), which was similar to a recipe of

additives noted in organotypic culture, where self-forming 3D retina from hESCs used 1% Matrigel and 10% FBS over 18 days (Nakano et al. 2012). We also compared MCF10A cells grown in 96 well U-bottom plates (H&E sections, Fig. 2a) and found greater hyperplastic regions within the lumens of the organoids in U-bottom plates compared to hanging drop organoids.

To further optimize the system, we explored organoid formation at varying concentrations of media-dissolved Matrigel over 3 days (Fig. 2b, Suppl. Fig. 1). In the absence of Matrigel, MCF10A forms highly compact spheres but were unable to differentiate beyond a cellular aggregate (Fig. 2c), 1% (*v*/v) Matrigel was the minimum concentration needed to observe differentiation, while increasing to 2% Matrigel rendered lower aggregate-forming ability. Thus, we achieved one large organoid per droplet at 95% forming efficiency using 1.5% Matrigel and 10% FBS over 3 days, an optimal recipe to establish uniform spheres. This is consistent with literature, in which FBS was shown to augment and enhance cellular differentiation (Nakano et al. 2012), while increasing Matrigel concentrations can decrease the number and function of acini formed (Lance et al. 2016).

We found by keeping cell seeding number and all other culture parameters constant, MCF10A organoid sizes increased by ~75% every 4 days for 16 days, co-culture and cancer organoids had slightly slower growth, while 10A MG^- spheres and EMT transformed organoids stopped proliferating after days 4 and 8, respectively (Fig. 2c). This suggests our cocktail of additives is critical for generating reproducible, uniform spheroids that can expand long-term, as shown by their range of sizes across cell subgroups (Fig. 2c), which has been a major challenge with conventional 3D platforms.

Available data suggest that hanging drop culture might provide advantages over other 3D spheroid assays for achieving organoid expansion. For example, conventional 3D gel embedded or on-top Matrigel culture of benign MCF10A acini (Vidi et al. 2013), and 3D microfluidic and PDMS microwell systems for cancer spheroids (Ziółkowska et al. 2012; Zhou et al. 2013) show significant restriction in size (<300 μm diameter) and proliferation potential, possibly due to mechanical confinement. Also, a recent study using microsensors found oxygen levels of multi-spheroids grown in conventional U-bottom 96 well plates dropped significantly after 18 h, while hanging drops containing one spheroid had stabilized oxygen values (Lesher-Pérez et al. 2017). Our observation of irregular morphologies, lumen filling, and no acini formation in 96 well U-bottom plates (Fig. 2a), suggests that hanging drops are organoid-supportive by providing more oxygen, by enhancing autocrine effects relative to the 96 well plates by using smaller media volumes, or by other unknown mechanisms.

We next investigated whether the expansion observed in MCF10A organoids may reflect a stem cell population since organoids described in literature are either propagated by stem cells (e.g. mammary progenitors, hESCs, iPSCs) or maintained by a known stem cell population. Western blot analysis of MCF10A organoids demonstrated the presence of a cell population with an EpCAM+/$CD49f^+$/$ALDH1^+$/$CD44^+$ stem cell phenotype (Suppl. Fig. 2). This is an important finding since previous studies of MCF10A cells in 3D Matrigel systems were not able to observe stem cell populations or reported a loss of stem/progenitor markers when moving from monolayer to 3D (Qu et al. 2015). These data suggest that the MCF10A cell line, in the absence of ECM scaffold, maybe maintained by a self-renewing stem/progenitor cell population in 3D culture allowing substantial expansion. This may be a potential advantage of growing cells in a free floatation context, whereby the investigation of stem cell populations over time can be readily monitored despite having less physiologically relevant ECM mimicry than typical 3D scaffold systems.

Organoids as models of neoplastic progression

We next compared the phenotypic features of normal MCF10A cells grown with and without Matrigel, and MDA-MB-231 breast cancer organoids in our model, noting similarities and differences with other 3D breast models (Lee et al. 2007; Klos et al. 2014; Mani et al. 2008; Fata et al. 2007; Anwar and Kleer 2013; Tran et al. 2011; Zhang et al. 2015; Naber et al. 2011). By day 8, MCF10A organoids develop a hollow lumen similar to acini (Debnath et al. 2003) but unlike typical acini embedded in an ECM gel, the organoids are able to grow (approximately 700 μm in diameter), and form a complex network of acini, resembling a normal human TDLU in tissues (Fig. 3, in vivo TDLU image, leftmost column; arrows indicate acinar structures). This contrasts with the limited 3D growth of MCF10A formed under suboptimal conditions (MG^-) which remain as cellular aggregates and do not exhibit tissue-specific markers (Fig. 3, middle column), and with MDA-MB-231 breast cancer organoids that display an invasive phenotype similar to that of invasive breast carcinoma in clinical tissue samples (Fig. 3, rightmost panel) (Pal and Kleer 2014). Over time, from day 4 through 16, MCF10A organoids undergo significant remodeling with lumen clearance, reduction of ECM matrix, and a tendency toward strict circular morphologies with increasingly cord-like basolateral peripheries (Suppl. Fig. 3A). Together, these results demonstrate that the hanging drop organoid system allows expansion of the cell populations with normal and neoplastic phenotypes, which can be applied to the study of breast tumorigenesis.

To directly test whether the MCF10A organoid platform in hanging drop is useful to study changes that occur during neoplastic progression, we subjected our model to different treatments shown to induce an epithelial-to-mesenchymal transition (EMT), an important process during tumorigenesis (Mani et al. 2008). MCF10A and other normal breast epithelial cells cultured in Matrigel were shown to undergo EMT and malignant transformation upon exogenous treatments

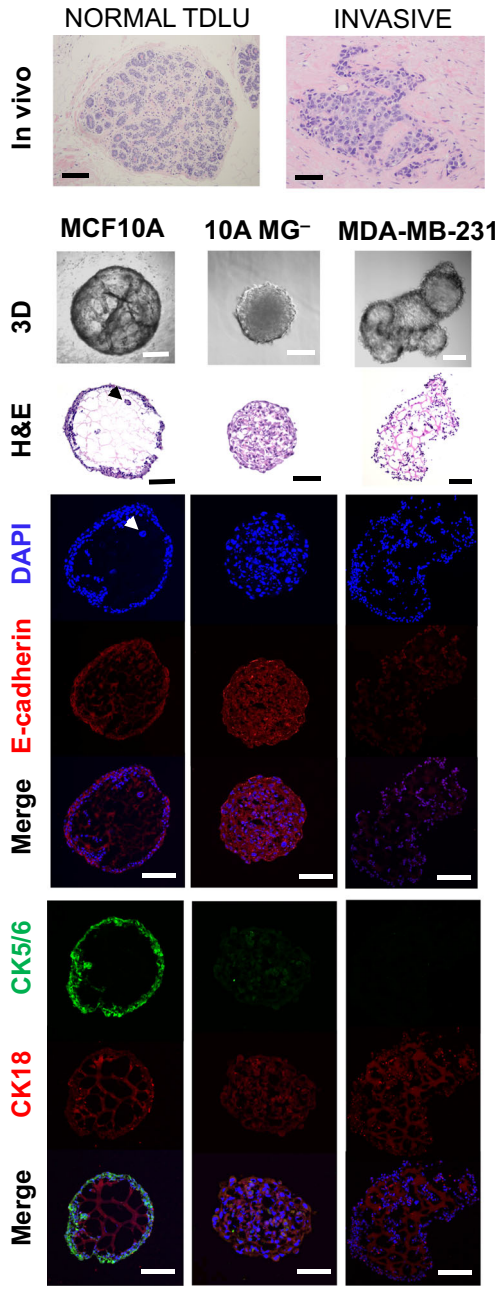

Fig. 3 Organoid formation with non-tumorigenic MCF10A, MCF10A Matrigel-free (MG⁻), and breast cancer MDA-MB-231 cells. Shown are representative images of the organoids at 8 days in 3D hanging drop with brightfield, H&E, and confocal images against Dapi, E-cadherin, CK5/6, and CK18. For comparison, images of a normal breast TDLU and an invasive ductal carcinoma from human tissues are shown with their characteristic morphology. Scalebar = 100 μm for 10A MG⁻ and 200 μm for all others. Black or white arrows indicate 3D acinar structures within organoids. Distinct phenotypic features of normal or invasive TDLU (top panel, in vivo histologic images) share phenotypic similarities with in vitro organotypic structures in 3D hanging drop culture for benign (MCF10A), tumorigenic or neoplastic (MDA-MB-231), and non-tissue-like cell mass (10A MG⁻) subgroups for the study of breast tumorigenesis and neoplastic progression

(Debnath et al. 2003; Klos et al. 2014; Fata et al. 2007), but whether these changes occur in scaffold-free 3D culture is unknown. We found that treatment of MCF10A organoids with TGFβ1 and the hypoxia mimetic agent, $CoCl_2$, two well established inducers of EMT and neoplastic transformation, led to a widespread loss of E-cadherin and increase in vimentin expression, which are hallmark responses of EMT (Fig. 4) (Anwar and Kleer 2013).

We selected treatment with TGFβ and the hypoxia-mimetic agent given their reported effect in induction of EMT and malignant transformation in breast cancer. Tests using TGFβ-induced transformation have been used more commonly in 2D MCF10A models (Tran et al. 2011; Zhang et al. 2015) than in 3D, with few reports utilizing a MCF10A gel-embedded system (Naber et al. 2011). Studies of hypoxia and MCF10A acini have been even fewer, in which hypoxia chambers were used, but these were unsuccessful in detecting EMT in MCF10A 3D culture (Vaapil et al. 2012). More recently, we found the literature points to certain chemical agents able to induce hypoxic effects rapidly, within minutes of administering, generating strong responses and higher controllability than hypoxia chambers (Mueller et al. 2009). Thus, we optimized a protocol using $CoCl_2$ induction from Wu and Yotnda (Wu and Yotnda 2011) and successfully generated rapid EMT-driven responses after just 24 h (Fig. 5a, H&E sections). For both TGFβ1 and $CoCl_2$ induction, we found significant deviation from normal MCF10A organoid morphology and signatures over days 8 through 16, with key differences highlighted in Supplemental Fig. 3B.

The ability to produce collagen and other ECM components has been ascribed to stromal cells (Zhu et al. 2014) and to cancer cells (Naba et al. 2012; Rizwan et al. 2015). Unexpectedly, we found that TGFβ and $CoCl_2$– induced a strong fibrotic-like response (Fig. 5a, Suppl. Fig. 3B, collagen I stains). Quantification of immunostaining results for TGFβ1 and $CoCl_2$ treated MCF10A organoids showed increased collagen I compared to untreated controls and were similar to levels observed in stromal cells and cancer cells (Fig. 5a, bottom plot). These data reveal the previously unknown ability of MCF10A cells to undergo de novo synthesis and deposition of collagen I upon EMT induction. Since conventional 3D gels often make use of collagen-containing matrices, the production of collagen from transformed normal epithelial cells would be an indiscernible or challenging feature to capture. The results indicate that benign breast cells such as MCF10A may have an inherent plasticity, which is revealed by using a gel-free culture platform. We also show that the de novo remodeling processes can be readily detected using H&E or IHC analyses. From a clinical translational perspective, the 3D organoid system can be applied to study ways to inhibit stromal fibrosis in cancer progression using pharmacological approaches.

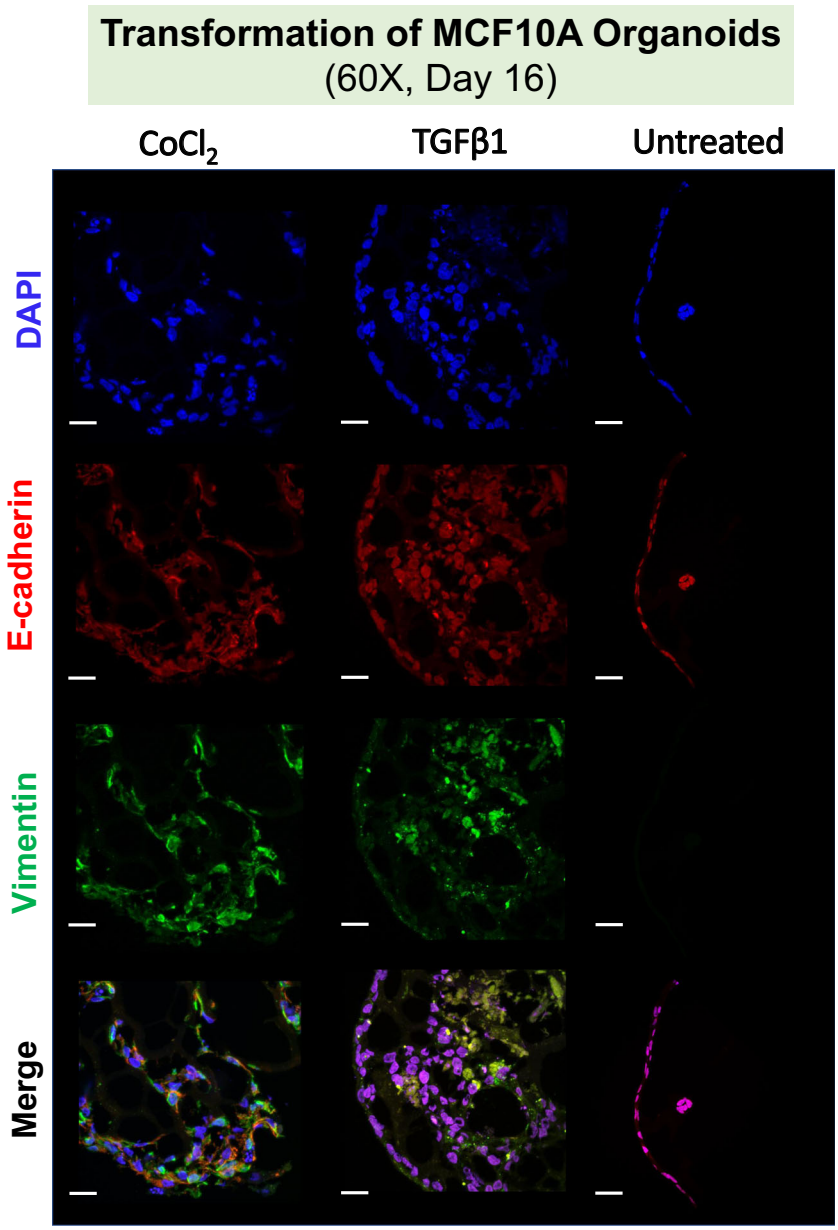

Fig. 4 Organoids as models of neoplastic progression. Epithelial-to-mesenchymal (EMT) induction assays were developed for the study of neoplastic transformation in MCF10A organoids by $CoCl_2$ and TGFβ1 treatment, two well-studied agents known to induce EMT and neoplastic progression of MCF10A cells. Representative confocal images captured at day 16 show altered expression of E-cadherin (red) and Vimentin (green) at 60X magnification in $CoCl_2$ and TGFβ1 treated organoids compared to normal expression in untreated MCF10A organoids. Scale bar = 25 μm. Neoplastic progression has not been explored in free floatation, scaffold-free 3D culture and allows organoids to be readily quantified using a 384-well HD format

Organoids allow epithelial-stromal cross-talk

The microenvironment consisting of stromal, immune, and vascular cells as well as structural ECM components has been shown to exert a powerful influence on breast cancer initiation and progression (Wang et al. 2017). Physiologically relevant in vitro models to study these interactions are needed. Towards this end, we generated a 3D heterotypic model with a simple test compartment of MCF10A and MSCs (Fig. 5b; MCF10A = blue, MSC = red).

Comparing to non-tumorigenic MCF10A organoids at day 8, co-culture organoids were significantly altered, with key features being disruption of CK5/6 expression, no acini formation, and lumen filling (Fig. 5b, H&E and confocal images). We also noted spindle-like MCF10A cell phenotypes and loss of cell-cell contact. These features reflect the influence of MSC-epithelial cell interactions, and suggest that the increased collagen output by MSCs may induce EMT on MCF10A cells (Fig. 5a, Suppl. Fig. 3B). This is consistent with studies from our lab, which showed that direct contact with MSCs induced a spindle morphology and increased migration and invasion of MCF10A cells through the collagen receptor DDR2 in co-culture experiments (Gonzalez et al. 2017). Our 3D organoid platform may be useful to study the details and consequences epithelial-stromal cross-talk during neoplastic initiation and progression and may offer an ideal system to test new therapies to block the stromal pro-tumorigenic influences on epithelial cells.

To investigate whether our new model can be used to grow fresh tumors, we set out to generate organoids derived from

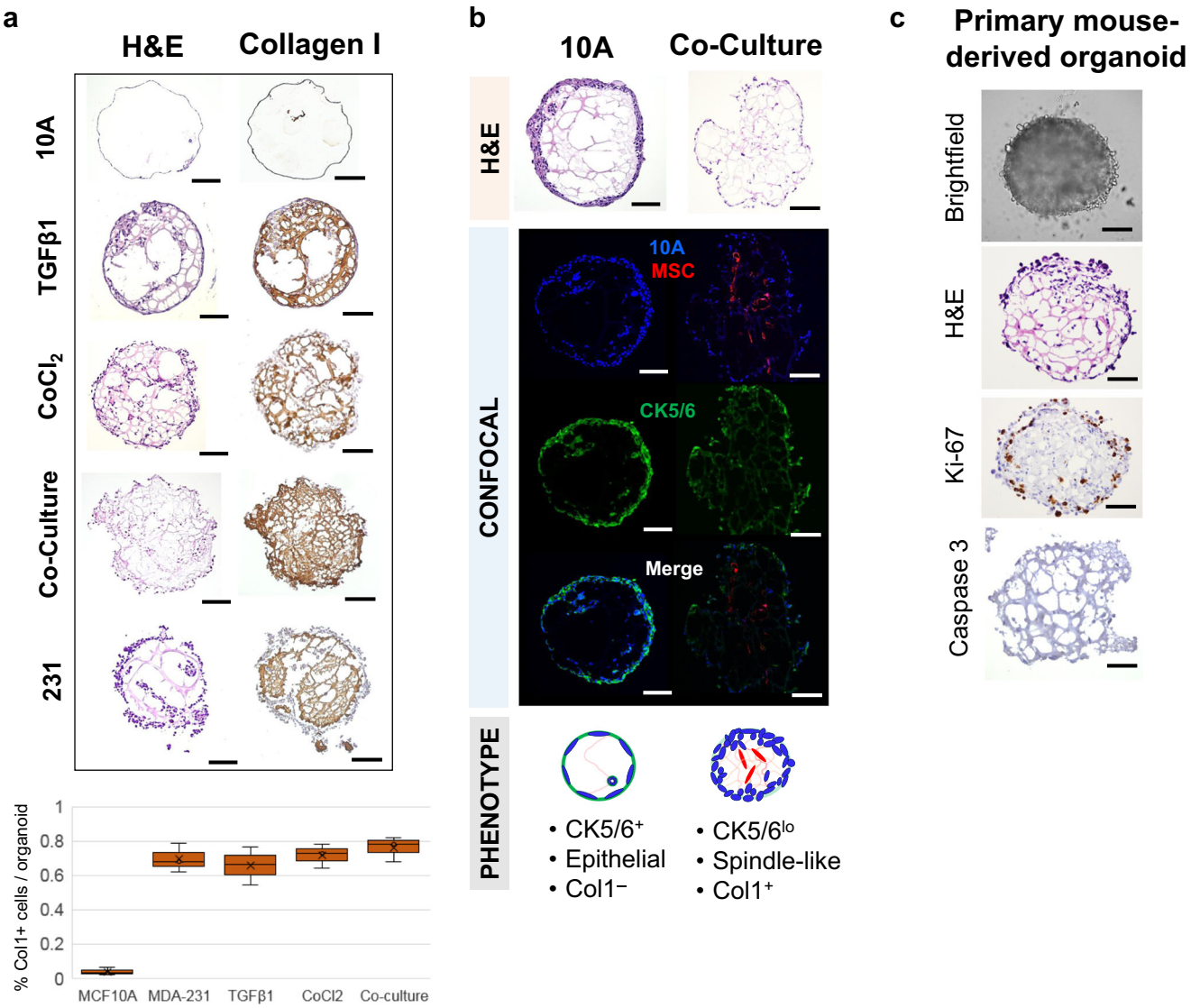

Fig. 5 Organoids developed in hanging drop exhibit phenotypic changes when subjected to different conditions and co-culture with MSCs. Phenotypes in organoids developed in hanging drop with **a**) collagen I profiles for MCF10A, TGFβ1, $CoCl_2$, co-culture, and MDA-MB-231 at day 16 ($N = 5$ per subgroup) compared with H&E and their associated fibrotic-like status via phenotypic quantitative analysis, **b**) H&E sections and confocal images at day 8 of non-tumorigenic MCF10A and co-culture organoids (MCF10A and MSCs seeded at a 1:1 ratio) showing spatial locations of MCF10A (blue) and MSC (red) cells within organoids, along with basal CK5/6 (green) status, and a schematic of typical morphology and phenotype based on epithelial/spindle-like features, or CK5/6 or Col1 expression, and **c**) MMTV-Cre;$Ccn6^{fl/fl}$ mouse mammary tumor-derived organoids with a live brightfield image at day 20, H&E and IHC sections for Ki67, and Cleaved Caspase 3. Scale bar = 200 μm

MMTV-Cre;$Ccn6^{fl/fl}$ mice, a breast cancer mouse model of metaplastic carcinomas developed in our lab (Martin et al. 2017) (Fig. 5c). The tumor-derived organoids contain spindle cancer cells similar to the primary originating tumors, and cells from the stromal and immune compartments. Methods for generating mouse mammary organoids in 3D culture have been limited, and typically describe propagation of epithelial organoids (Sato et al. 2011). In addition, we demonstrate detectable protein expression (e.g. proliferation marker Ki67 and apoptotic marker cleaved caspase 3). Because of growing interest in patient tumor derived organoids for purposes of biobanking (Wetering et al. 2015) and single cell sequencing (Chung et al. 2017), these efforts have mainly focused on the primary epithelial compartment, but there is a great need to expand our understanding of patient intratumoral heterogeneity analyses. Our results of mouse tumor-derived organoids show a step in that direction, forming in a highly reproducible format over shorter time periods.

Overall, the two major substrata used in 3D breast models, collagen I gels and Matrigel, are essential for providing the context whereby systemic cues can mimic the microenvironment, such as directing gene expression and cell responses (Bissell et al. 1982). But there are no specific guidelines for 3D systems on how best to mimic particular features of the

in vivo situation (Thoma et al. 2014). Although use of a scaffold can preserve MCF10A acinar mechanical integrity by reproducing pressure forces like those found in vivo (Gaiko-Shcherbak et al. 2015), spheroids grown under free suspension may not experience similar pressure cues, which could be a potential drawback. The lack of ECM biophysical forces could explain why MCF10A organoids undergo substantial expansion to approximately twenty-five times the size of normal breast acini. Even though as a structural unit, they are larger than the reported in vivo range, their ability to expand highlights a tight cellular commitment to the normal morphogenetic program.

Moreover, a major disadvantage of gel systems is their restricted ability to express tissue-specific markers (Emerman and Pitelka 1977). Our data support the idea that a 3D free-floatation context might provide a more permissive environment for differentiation as previously stipulated (Marina and Bissell 2017). Thus, a general guideline for investigators using scaffold or suspension systems is to consider the relevant biophysical and spatiotemporal factors to facilitate a desired outcome.

Assessment of morphologic and phenotypic parameters of normal and neoplastic progression in organoids

Despite an increase in studies using 3D tumor models in recent years, there remains a lack of standardization in spheroid and organoid analyses. Some investigators advised monitoring a combination of morphological parameters (Kelm et al. 2003; Celli et al. 2014; Zanoni et al. 2016) such as volume, sphericity, and area, however this information can be quite variable in the literature, stemming from inconsistencies in reproducibility and uniformity. More recently, Reid and others developed a highly consistent and reproducible mammary organoid bioprinting method to better standardize the analysis of 3D cultures (Reid et al. 2018). Therefore, it is important to use a quantifiable metric to link our "observables" to biological relevance. With this outlook, we performed morphometric analyses on organoid parameters for average diameter, sphericity, hollowness, and phenotypic analyses on epithelial-like (E-cadherin+), mesenchymal-like (spindle +), basal / progenitor (CK5/6+), and fibrotic-like (Col1+) features for all tested organoid subgroups, i.e. non-tumorigenic (MCF10A), tumorigenic (MDA-MB-231), and neoplastic (co-culture, $CoCl_2$, TGFβ1) (Fig. 6).

ANOVA tests performed across all culture conditions for organoid-level morphologic and cellular-level phenotypic parameters at days 8 and 16 were statistically highly significant ($P < 0.001$) (Fig. 6a). We found from days 8 to 16, sphericity and hollowness had diverged across conditions resulting in decreased P-values ($P < 1E-06$). Since tumorigenic and non-tumorigenic morphologic parameters become well distinguished at 16 days, this suggests sphericity and hollowness could be suitable biological indicators for analyzing dynamic changes in organoids in short-term culture. Others have also noted overall shape is a highly variable parameter yet crucial indicator of tumorigenicity, as in a recent study that examined over 100 primary breast cancer organoid lines (Sachs et al. 2018). The improved significance over time suggests when looking for distinct morphologic traits in organoids, they should be cultured >2 weeks.

On the other hand, all cell phenotypic features were distinct by day 8 for all organoid subgroups (P < 1E-08) (Fig. 6a). For neoplastic organoids, mesenchymal and fibrotic-like features converged to a tumorigenic phenotype just 2 days after treatment, with increased P-values at day 16 ($P = 0.005$ and $P = 0.19$, respectively), becoming phenotypically indistinguishable to MDA-MB-231 organoids. Thus, although organoid phenotypes are statistically unique, upon neoplastic progression they become harder to distinguish. As a result, we observed that epithelial and basal traits were harder to decipher since over time significances did not change as much as mesenchymal and fibrotic-like traits in response to a treatment. In relating phenotype to morphology, we found organoid sizes <400 μm in general do not display organotypic expansion or differentiation (e.g. 10A MG– 3D structures), whereas after organoids reached >800 μm in diameter, we detected unique multi-phenotypic and multi-morphologic states, summarized in the Fig. 6b table. Here, sphericity/lm status provided approximate regimes as follows: a normal epithelial, non-fibrotic state (> 0.75), a mesenchymal, fibrotic-like "invasive" state with largely filled lumen (< 0.5), and a mixed phenotype "irregular" regime (0.5–0.75) reflecting all neoplastic states (e.g. EMT, cancer, heterotypic).

Highly-reproducible evaluation of 3D organoids may be used in future experiments using patient-derived tumor specimens, to facilitate the study of large-scale drug screening and patient organoid biobanking (Weeber et al. 2017). We advise a quantitative analytical assessment based on a combination of morphological and phenotypic parameters for 3D tumor models, outlined in the Fig. 6b table, which can be applied across cell types and conditions. In relating morphology with phenotype, filled lumen status and fibrotic-like features of neoplastic organoids could reflect an ability to produce their own ECM which normal epithelial cells clearly lacked. However, those more difficult to discern traits such as basal / progenitor status, which might drive organoid regeneration, suggest an underlying mechanistic complexity to be followed up in future studies. Our model offers important advantages over previous organoid and 3D embedded culture methods, which are summarized in Table 1.

In summary, the present work describes a non-embedded, gel-free, hanging drop culture that enabled consistent production of highly-spherical MCF10A non-tumorigenic breast organoids with surprisingly large diameters in good yield. We further developed neoplastic organoids also with uniform, reproducible sizes and shapes, facilitating standardization

a

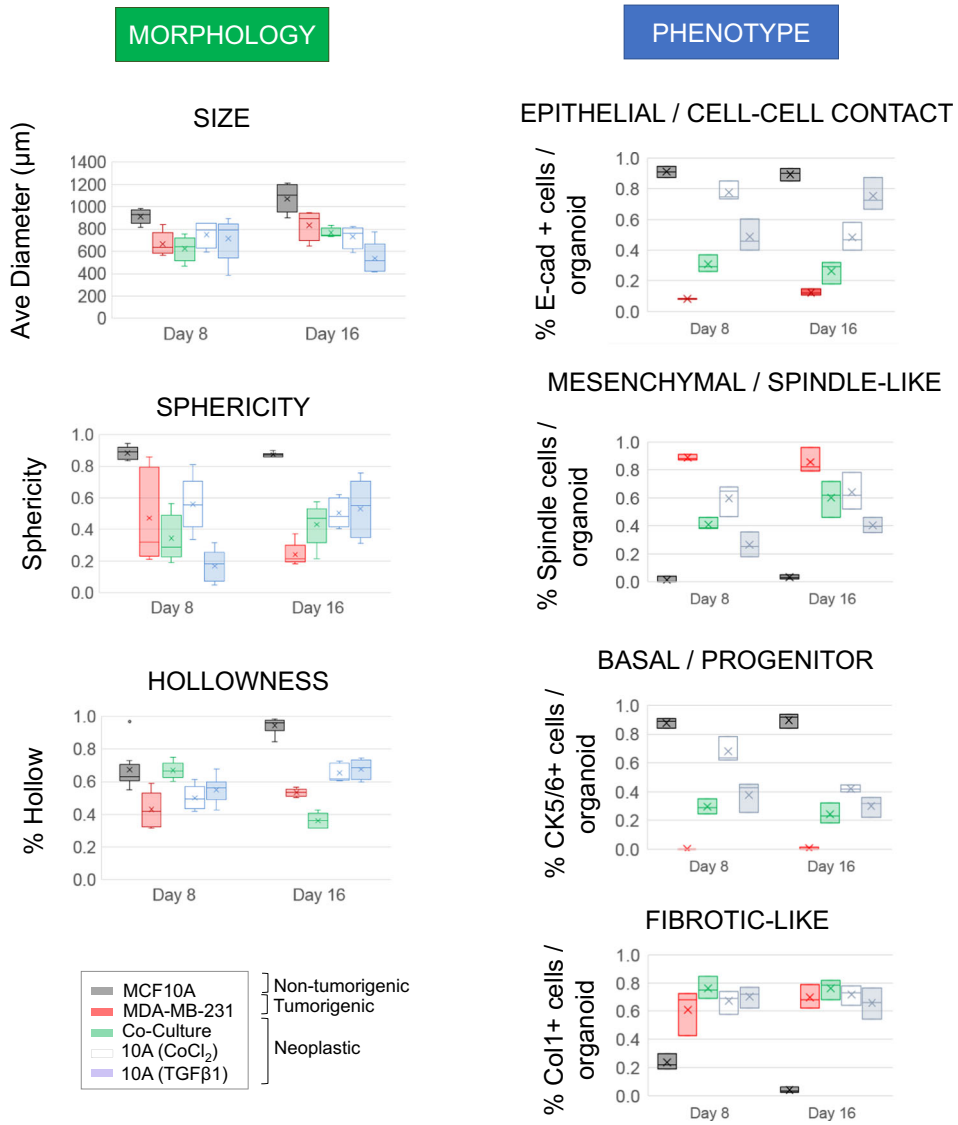

b

Cell Type	MORPHOLOGIC PARAMETERS			PHENOTYPIC PARAMETERS			
	Size (Ave Diameter, µm)	Shape* (Sphericity)	Lumen† (Hollowness)	Epithelial / cell-cell contact	Mesenchymal / spindle-like	Basal or progenitor	Fibrotic-like
MCF10A	1070±105	spherical (0.87-0.90)	hollow (0.91-0.98)	++	–	++	–
MDA-MB-231	835±115	irregular (0.19-0.30)	filled (0.51-0.56)	–	++	–	++
Co-culture	765±40	irregular (0.22-0.58)	filled (0.32-43)	+	++	+	++
$CoCl_2$ treated	755±90	semi-spherical (0.41-0.61)	partial filled (0.61-0.74)	++	+	+	++
TGFβ1 treated	540±130	semi-spherical (0.35-0.71)	partial filled (0.61-0.72)	++	+	+	++

against other parameters. The obtained MCF10A organoids contain cells of multiple phenotypic lineages including tissue-specific and progenitor-like populations mimicking signatures of normal TDLUs. When exposed to conditions that mimic neoplastic progression, the organoids underwent cellular-level phenotypic changes and organoid-level morphologic changes that could be quantified to stratify organoid responses. The one droplet – one organoid simplicity, the highly regular shape and size of the obtained organoids, and dramatic morphologic changes upon exposure to neoplastic

◀ **Fig. 6 Evaluation of organoid morphologic and phenotypic parameters. a**) Morphology parameters: average organoid diameter, sphericity, and hollowness, and phenotype parameters: epithelial/cell-cell contact (E-cadherin+), mesenchymal-like (spindle-like+), basal/progenitor (CK5/6+), and fibrotic-like (Collagen I+). Phenotypic parameters were based on the percentage of positive stained cells per organoid (N = 5 organoids per subgroup, triplicated, 75–150 cells analyzed per section). Organoids were categorized as non-tumorigenic (MCF10A), tumorigenic (MDA-MB-231) and neoplastic (co-culture, TGFβ1 and $CoCl_2$ treated). **b**) table of the combined morphologies and phenotypes represented in a table showing results of quantitative measurements of all organoid subgroups at day 16. For morphologic parameters (N = 10 per group): * = Sphericity >0.75 on scale of [0–1] is "spherical," < 0.5 is "irregular," and ~ 0.5–0.75 is "semi-spherical". † = % Hollowness >0.75 is "hollow," 0.5–0.75 is "partial filled," and < 0.5 is "filled," where "–" indicates no observed expression, "++" indicates a percentage of positive cells per organoid >50%, and "+" indicates percent positive cells <50%

conditions open the door for assay standardization and high-throughput testing.

Methods

Cell lines and cell culture MCF10A and MDA-MBA-231 cell lines were obtained from the American Type Culture Collection (Manassas, VA). MCF10A, an immortalized non-transformed human breast epithelial cell line, is a well-established in vitro model of the benign breast. MCF10A are near-diploid cells with stable karyotype. MCF10A cells were cultured in growth medium containing DMEM/F12 (Invitrogen #11965–118), Horse serum (Invitrogen #16050–122) and supplements as previously reported by Debnath and colleagues (Debnath et al. 2003) and MDA-MB-231 cells were maintained as per the manufacturer's instructions with culture medium composed of DMEM (Invitrogen) supplemented with 10% Fetal Bovine Serum (FBS). DsRed-labeled mesenchymal stem cells (MSCs) were generated by the Kleer Lab (Gonzalez et al. 2017), where MSCs were isolated from fresh human breast cancer metastasis tissue (The Tissue Procurement Service at the University of Michigan, IRB#HUM00050330). MSCs were maintained as reported by Gonzalez et al. (Gonzalez et al. 2017). All cells were cultured at 37 °C and 5% CO_2 in 100 mm culture dishes, supplemented with 1% antibiotic-antimycotic, passaged before ~75% confluence was reached, and monitored with brightfield images collected at 10x magnification.

3D culture A hanging drop array system was used to generate high-throughput 3D organoid culture in a 384-well format (Tung et al. 2011). Hanging drop plates were coated in 0.1% Pluronic F108 (BASF) and UV sterilized. Hanging drops were formed using cell suspension solution with optimized media additives (Leung et al. 2015), 0.24% (*w*/*v*) methylcellulose (A4M MethoCel, Dow Chemical, MI) and 1.5–2% (*v*/v) Matrigel (growth factor reduced, phenol red-free, BD Biosciences, #356231), where 25 μl droplets were maintained. MCF10A cells were seeded at a density of 3000 cells per droplet, MDA-MB-231 cells were seeded at 2000 cells per droplet, and co-cultures with MCF10A and MSC cells were seeded at 1:1 with 2000 total cells per droplet. To avoid evaporation, the array plate was sandwiched between a 96-well plate (Corning Costar 3596, Corning Inc., Lowell, MA) and plate lid to create a humidified environment. Fresh media was replenished every 2–3 days using a liquid handler (CyBi-Well, CyBio, Inc., Jena, Germany). Approximately 8–9 μl solution was removed from a drop and 9–10 μl fresh media added into a drop, repeated twice. For MCF10A organoids, we also added 10% FBS to the seeding solution to enhance organoid growth, and after spheres formed at day 3, we removed Matrigel, FBS, and MethoCel from the droplets with ~3 washes and replaced with complete media (Debnath et al. 2003; Leung et al. 2015) for the duration of culture. All organoids were maintained for 16 days and monitored by phase-contrast imaging (Nikon Eclipse TE300 inverted microscope). For comparison, MCF10A cells were seeded and maintained in a 96-well 3D format using the exact same parameters as in 3D hanging drop cultures except using 100 μl volumes and for media changes, 32 μl was removed from wells and replaced with 34 μl fresh media during each wash.

3D epithelial-to-mesenchymal (EMT) induction assays Epithelial-to-mesenchymal induction assays were performed in the hanging drop system using MCF10A cells treated exogenously with either human recombinant TGF-β1 (Sigma, GF346) or a hypoxia mimetic, $CoCl_2$ (Cobalt(II) Chloride 97%, Sigma, 232,696). TGF-β1 and $CoCl_2$ solutions were prepared following manufacturer's instructions. For TGF-β1 induction assays, MCF10A organoids were grown for 5 days in hanging drop plates, followed by serum starvation of the droplets for 16 h using serum-free DMEM/F12 medium (Invitrogen #11330–032). TGF-β1 was added to the serum-free medium, and a final concentration of 10 ng/ml TGF-β1 was added to droplets upon media exchanges and replenished after 2 days. Organoids were exposed to TGF-β1 for 4 days and removed from droplets with 7–8 washes of complete medium. For another 6 days, organoids were grown with complete medium and harvested from the plates. For $CoCl_2$ assays, hypoxia induction was performed as previously reported (Wu and Yotnda 2011). MCF10A organoids were grown as usual for 5–6 days. $CoCl_2$ was added directly to regular complete medium to induce a hypoxia-like response at a final concentration of 100 μM $CoCl_2$ for 24 h. $CoCl_2$ was removed with 7–8 washes of complete medium, and organoids were allowed to grow for another week before harvesting.

Cryoblock embedding and sectioning Organoid samples were collected from the array plate at a desired time, rinsed once

Table 1 Advantages of scaffold-free organoids to study neoplastic progression over other 3D methods

Cell culture system	Advantages and Applications	Disadvantages	References
Conventional scaffold-based 3D culture	• In vivo-like 3D organization compared to 2D cultures • Physiologic microenvironments • Direct cell-ECM interactions, biophysical responses • Luminal and basal marker expression • Long-term culture, easily maintained	• Highly variable 3D structures and variable differentiation capacity • Low throughput • Difficult to access aggregates • Limited modeling tumorigenic signaling • Mass transfer barriers • Potential loss of stem/progenitor populations	(Barcellos-Hoff et al. 1989) (Petersen et al. 1992) (Debnath et al. 2003) (Lee et al. 2007) (Pal and Kleer 2014)
Scaffold-free hanging droplet	• Single organoid per droplet, high-throughput, high reproducibility, compact aggregates • Direct cell-cell interaction • Ideal for modeling tumorigenic signaling over time • Maintains stem/progenitor expression • Easily quantifiable tumorigenicity status • Multipotent phenotypic differentiation of breast cells • Well suited for primary tumor organoids • Rapid testing of pharmacological interventions • In vivo-like microenvironment and cell-ECM interaction when derived from primary cultures	• Lack of in vivo microenvironment and cell-ECM cues when derived from cell lines • Difficulty to maintain long-term • Risk of droplet dehydration or mechanical disruption • Time consuming and/or labor intensive	This study
Hanging droplet (our previous work)	• High-throughput, compact spheres, simple usage • Scaffold-free, easy manipulation of droplets • Single tumor spheroids per droplet by gravity • Rapid testing with various therapeutics, easy media changes and access	• Unable to generate spheres from normal breast cells • Limited differentiation, variable 3D aggregates • Lack of standardization approach	(Tung et al. 2011) (Leung et al. 2015)

with 1x PBS (GIBCO #10082), fixed in 4% PFA solution for 2 h at room temperature, and washed again three times in 1x PBS. Prior to embedding, fixed organoids were stained with 0.1% (*v*/v) methylene blue for 10 min and rinsed with PBS. Next, a thin layer of optimal cutting temperature (OCT) compound (Tissue-Tek, Sakura Finetek, CA, #4583) was placed into a 5 × 5 mm cryomold, and the desired number of organoids were pipetted into the OCT layer. Additional OCT was filled to the top of the cryomold and snap-frozen on dry-ice, in block form, for 10 min in a Styrofoam container. The frozen blocks were stored at −80 °C, and subsequently sectioned into 5 μm sections on a Lecia 3050S Cryostat (Leica Biosystems Inc., IL) and mounted onto slides for staining.

H&E and immunohistochemistry (IHC) After thawing for 5 min, slides with sectioned organoids were rehydrated with 1X TBS buffer for 10 min. Heat induced epitope retrieval was performed with FLEX TRS Low pH Retrieval buffer (6.1, Dako, Carpinteria, CA) for 20 min. After peroxidase blocking, the antibody Collagen 1 rabbit polyclonal (Abcam, #ab34710) was applied at a dilution of 1:500 at room temperature for 60 min. The EnVision + Rabbit HRP System was used for detection. DAB chromagen was then applied for 10 min. Slides were counterstained with Harris' Hematoxylin and Eosin (H&E) for 5 s and then dehydrated and coverslipped. For mouse-derived organoids, primary antibodies used included Ki67 and Cleaved Caspase 3. Ki-67 rabbit monoclonal (Cell Marque, SP6 #475 R-16, Rocklin, CA) was applied at a dilution of 1:250 at room temperature (R.T.) for 30 min, and Cleaved Caspase-3 rabbit polyclonal (Cell Signaling #9661, Danvers, MA) at a dilution of 1:300 at R.T. for 60 min. To compare with organoid sections, we prepared H&E sections on human breast tissues samples obtained from University of Michigan (IRB approval HUM00050330).

Immunofluorescence and confocal imaging Sectioned organoids were immediately fixed in 70% (*v*/v) methanol and stored at −20 °C. After fixation, blocking of nonspecific binding of the antibodies was accomplished by incubation with Background Sniper (BioCare Medical, Pacheco, CA) for 30 min, followed by incubation overnight at 4 °C with pairs of primary antibodies (mouse and rabbit). Primary antibodies included anti-E-cadherin (1:100, mouse monoclonal antibody, clone HECD-1, Thermo Fisher Scientific, Waltham MA, 13–1700), anti-CK5/6 (1:100, Thermo Fisher Scientific, Mouse monoclonal antibody, clone D5/16 B4), anti-CK18 (1:100, Rabbit monoclonal antibody clone ER431–1, AbCam, Cambridge, Ma, Ab32118), and anti-Vimentin (1:300, Rabbit monoclonal antibody, clone EPR868 (Petersen et al. 1992), AbCam, Ab133260). After washing with Tris buffered saline (10 mM Tris HCl, pH 7.4/ 0.154 M NaCl) containing 0.1% Tween 20 (TBST), the slides were incubated with fluorescent-conjugated secondary antibodies Cy3 and Cy5 for 30 min (1:200, #A10520–21, #A10523–24, Thermo Fisher

Scientific) diluted in background sniper. After additional washes with TBST, sections were mounted using Prolong Gold (Thermo Fisher Scientific) containing 4′,6-diamidino-2-phenylindole (DAPI) and confocal images were captured with a Nikon A-1 Spectral Confocal microscope using a 20X and 40X oil objective.

Western blot Cells were collected and subsequently lysed in RIPA lysis buffer with protease and phosphatase inhibitors (Thermo Scientific #78410) at 100x dilution. Western blots were performed using 40 μg of total protein, separating the protein samples by SDS-PAGE gel and transferring onto PVDF membranes. The membranes were blocked in TBS-T (Tris-buffered saline, 0.1% Tween 20) and 5% milk, and then incubated with primary antibodies in TBS-T at 4 °C overnight. Abcam antibodies: CD49f (#AB112181), Vimentin (#AB16700), CD44 (#AB51037). Cell Signaling antibody: E-cadherin (#3195). Thermo Fisher antibodies: ALDH1A1 (#PA5–11537), EpCam (#710524). B-Actin-HRP (Santa Cruz, #47778) was used as a loading control.

Mouse-derived organoids of MMTV-Cre;*Ccn6*$^{fl/fl}$ mammary tumors (CCN6 KO) CCN6 KO tumors from genetically engineered mice developed in the Kleer lab (Martin et al. 2017) were dissociated into tissue fragments and single cells prior to organoid generation. Tumor samples were washed for 5 min in 1x PBS, pH 7.4, then manually cut into small fragments (>1 mm diameter) with a scalpel, tissue fragments were mechanically and enzymatically dissociated into a single-cell suspension using the MACS Tumor Dissociation Kit- mouse (Cat# 130–096-730, Miltenyi Biotec). After centrifugation and media aspiration, the remaining tumor cells together with the cancer-associated stroma were resuspended in suspension media containing DMEM, 1x B27, 1x insulin transferrin selenite ethanolamine, 1x non-essential amino acids, EGF (10 ng/ml), bFGF (10 ng/ml), and 1x antibiotics. The cell suspension was then used to perform 3D hanging-drop culture as previously described. After 20 days, mouse-derived organoids were harvested, embedded, and sectioned as described above.

Morphological metrics and phenotypic assessment Image processing for all morphological parameters was done in ImageJ software using the Watershed algorithm and binarization techniques as previously discussed (Roerdink and Meijster 2000). The morphological parameters average organoid diameter, sphericity, and hollowness were measured by standard image segmentation techniques in ImageJ software using adaptive thresholding with the Watershed algorithm and binarization to create a mask of organoid boundaries. Morphological features were measured in triplicate with $N = 10$ organoids for each group of cells and conditions, as indicated. Best fit ellipsoids of irregular organoid shapes were determined for average diameter and sphericity measurements using Feret's statistical diameter as an approximated equivalent diameter. Sphericity (named "circularity" in ImageJ) was measured as a ratio between 0 to 1, 1 being a perfect circle. The % hollowness was determined as a ratio of total area of cell and matrix regions to total organoid bounding area. For phenotype quantification, we measured the percentage of positive cells per organoid section by manual counting. This was calculated using threshold adjusted immunofluorescence signals from a Nikon E-800 microscope, with $N =$ 75–150 cells per organoid section and $N = 5$ organoids per subgroup, and the results were triplicated. Similarly, we counted spindle-like cells in the same manner using H&E sections and confocal DAPI images.

Statistical analysis Results were expressed as means ± standard deviations and statistical analysis was performed using one-way ANOVA tests for morphologic and phenotypic data at days 8 and 16. Statistical significances of $P < 0.05$ and highly significant $P < 0.001$ results were considered. At each time point, ANOVA tests were carried out between non-tumorigenic (MCF10A), tumorigenic (MDA-MB-231) and neoplastic (co-culture, $CoCl_2$, TGFβ1) organoid subgroups.

Acknowledgements We thank Tina Fields (Research Histology and IHC Laboratory, Rogel Cancer Center, University of Michigan) and Dafydd Thomas (Department of Pathology, Michigan Medicine) for their assistance with sectioning, immunohistochemistry, and immunostaining procedures and Dr. Brendan Leung for early studies. The study was supported by R01 grants to Dr. Celina Kleer (R01 CA107469, R01 CA125577, and the Karlene Kulp Fund Judy & Ken Robinson Fund), Dr. Shuichi Takayama (R01 CA196018), and the University of Michigan Rogel Cancer Center support grant P30CA046592. The authors would also like to thank Dr. Alexey Nesvizhskii for continued support by the Proteome Informatics of Cancer Training Program (PICTP) (NIH 5T32CA140044-08).

Author contributions S.D., C.K., and S.T. were involved in the study conception, design, analyses and interpretation. S.D. performed data acquisition and analysis, and B.B. and M.M. helped with completion of experiments and interpretation. S.D. prepared the manuscript and figures, C.K. and S.T. helped with the revision of the manuscript. All authors read and approved the final manuscript.

Data availability The raw/processed data required to reproduce these findings cannot be shared at this time as the data also forms part of an ongoing study.

Compliance with ethical standards

Competing financial interests The authors declare no competing financial interests.

Publisher's Note Springer Nature remains neutral with regard to jurisdictional claims in published maps and institutional affiliations.

References

Abd El-Rehim DM et al (2004) Expression of luminal and basal cytokeratins in human breast carcinoma. J Pathol 203:661–671

Aijian AP, Garrell RL (2015) Digital microfluidics for automated hanging drop cell spheroid culture. J Lab Autom 20:283–295

Anwar TE, Kleer CG (2013) Tissue-based identification of stem cells and epithelial-to- mesenchymal transition in breast cancer. Hum Pathol 44:1457–1464

Barcellos-Hoff MH, Aggeler J, Ram TG, Bissell MJ (1989) Functional differentiation and alveolar morphogenesis of primary mammary cultures on reconstituted basement membrane. Development 105: 223–235

Bissell MJ, Hall HG, Parry G (1982) How does the extracellular matrix direct gene expression. J Theor Biol 99:31–68

Boecker W, Buerger H (2003) Evidence of progenitor cells of glandular and myoepithelial cell lineages in the human adult female breast epithelium: a new progenitor (adult stem) cell concept. Cell Prolif 36(Suppl 1):73–84

Celli JP et al (2014) An imaging-based platform for high-content, quantitative evaluation of therapeutic response in 3D tumour models. Sci Rep 4:1–10

Cerchiari AE et al (2015) A strategy for tissue self-organization that is robust to cellular heterogeneity and plasticity. Proc Natl Acad Sci 112:2287–2292

Chandler EM et al (2011) Stiffness of photocrosslinked RGD-alginate gels regulates adipose progenitor cell behavior. Biotechnol Bioeng 108:1683–1692

Chung W et al (2017) Single-cell RNA-seq enables comprehensive tumour and immune cell profiling in primary breast cancer. Nat Commun 8

Debnath J, Muthuswamy SK, Brugge JS (2003) Morphogenesis and oncogenesis of MCF-10A mammary epithelial acini grown in three-dimensional basement membrane cultures. Methods 30:256–268

Emerman J, Pitelka DR (1977) Maintenance and induction of morphological differentiation in dissociated mammary epithelium on floating collagen membranes. In Vitro 13:316–328

Fata JE et al (2007) The MAPKERK-1,2pathway integrates distinct and antagonistic signals from TGFα and FGF7 in morphogenesis of mouse mammary epithelium. Dev Biol 306:193–207

Gaiko-Shcherbak A et al (2015) The acinar cage: basement membranes determine molecule exchange and mechanical stability of human breast cell acini. PLoS One 10:1–20

Gonzalez ME et al (2017) Mesenchymal stem cell-induced DDR2 mediates stromal-breast Cancer interactions and metastasis growth. Cell Rep 18:1215–1228

Gusterson BA, Ross DT, Heath VJ, Stein T (2005) Basal cytokeratins and their relationship to the cellular origin and functional classification of breast cancer. Breast Cancer Res 7:143–148

Kelm JM, Timmins NE, Brown CJ, Fussenegger M, Nielsen LK (2003) Method for generation of homogeneous multicellular tumor spheroids applicable to a wide variety of cell types. Biotechnol Bioeng 83: 173–180

Klos KS et al (2014) Building bridges toward invasion: tumor promoter treatment induces a novel protein kinase C-dependent phenotype in MCF10A mammary cell acini. PLoS One 9:1–11

Lance A et al (2016) Increased extracellular matrix density decreases MCF10A breast cell acinus formation in 3D culture conditions. J Tissue Eng Regen Med 10:71–80

Lee GY, Kenny P a, Lee EH, Bissell MJ (2007) Three-dimensional culture models of normal and malignant breast epithelial cells. Nat Methods 4:359–365

Lesher-Pérez SC et al (2017) Dispersible oxygen microsensors map oxygen gradients in three-dimensional cell cultures. Biomater. Sci. 5: 2106–2113

Leung BM, Lesher-Perez SC, Matsuoka T, Moraes C, Takayama S (2015) Media additives to promote spheroid circularity and compactness in hanging drop platform. Biomater Sci 3:336–344

Linnemann JR et al (2015) Quantification of regenerative potential in primary human mammary epithelial cells. Development 142: 3239–3251

Mani SA et al (2008) The epithelial-mesenchymal transition generates cells with properties of stem cells. Cell 133:704–715

Marina S, Bissell MJO (2017) A historical perspective of thinkin in three dimensions. J Cell Biol 216:1–10. https://doi.org/10.1083/jcb.201610056

Martin EE, Huang W, Anwar T, Arellano-Garcia C, Burman B, Guan J-L, Gonzalez ME, K CG (2017) MMTV-cre;Ccn6 knockout mice develop tumors recapitulating human metaplastic breast carcinomas. Oncogene 36:2275–2285

Mueller S, Millonig G, G W (2009) The GOX/CAT system: a novel enzymatic method to independently control hydrogen peroxide and hypoxia in cell culture. Adv Med Sci 54:121–135

Naba A, Hoersch S, Hynes RO (2012) Towards definition of an ECM parts list: an advance on GO categories. Matrix Biol 31:371–372

Naber HPH, Wiercinska E, ten Dijke P, van Laar T (2011) Spheroid assay to measure TGF-β-induced invasion. J Vis Exp:e3337. https://doi.org/10.3791/3337

Nakano T et al (2012) Self-formation of optic cups and storable stratified neural retina from human ESCs. Cell Stem Cell 10:771–785

Pal A, Kleer CG (2014) Three dimensional cultures: A tool to study normal acinar architecture vs. malignant transformation of breast cells. J Vis Exp:e51311. https://doi.org/10.3791/51311

Pal A, Huang W, Toy KA, Kleer CG (2012) CCN6 knockdown disrupts acinar Organization of Breast Cells in three-dimensional cultures through up-regulation of type III TGF-β receptor. Neoplasia 14: 1067–1074

Petersen OW, Ronnov-Jessen L, Howlett AR, Bissell MJ (1992) Interaction with basement membrane serves to rapidly distinguish growth and differentiation pattern of normal and malignant human breast epithelial cells. Proc Natl Acad Sci 89:9064–9068

Qu Y et al (2015) Evaluation of MCF10A as a reliable model for normal human mammary epithelial cells. PLoS One 10:1–16

Quadrato G et al (2017) Cell diversity and network dynamics in photosensitive human brain organoids. Nature 545:48–53

Reid JA, Mollica PM, Bruno RD, Sachs PC (2018) Consistent and reproducible cultures of large-scale 3D mammary epithelial structures using an accessible bioprinting platform. Breast Cancer Res 20:1–13. https://doi.org/10.1186/s13058-018-1045-4

Rizwan A et al (2015) Metastatic breast cancer cells in lymph nodes increase nodal collagen density. Sci Rep 5:1–6

Roerdink J, Meijster A (2000) The watershed transforms: definitions, algorithms and parallelization strategies. Fundam Inform 41(1-2): 187–228. https://doi.org/10.3233/FI-2000-411207

Sachs N et al (2018) A living biobank of breast Cancer organoids captures disease heterogeneity. Cell 172:373–386.e10

Sato T et al (2011) Long-term expansion of epithelial organoids from human colon, adenoma, adenocarcinoma, and Barrett's epithelium. Gastroenterology 141:1762–1772

Simian M et al (2001) The interplay of matrix metalloproteinases, morphogens and growth factors is necessary for branching of mammary epithelial cells. Development 128:3117–3131

Thoma CR et al (2013) A high-throughput-compatible 3D microtissue co-culture system for phenotypic RNAi screening applications. J Biomol Screen 18:1330–1337

Thoma CR, Zimmermann M, Agarkova I, Kelm JM, Krek W (2014) 3D cell culture systems modeling tumor growth determinants in cancer target discovery. Adv Drug Deliv Rev 69–70:29–41

Tran DD, Corsa CAS, Biswas H, Aft RL, Longmore GD (2011) Temporal and spatial cooperation of Snail1 and Twist1 during epithelial-mesenchymal transition predicts for human breast Cancer recurrence. Mol Cancer Res 9:1644–1657

Tung Y-C et al (2011) High-throughput 3D spheroid culture and drug testing using a 384 hanging drop array. Analyst 136:473–478

Vaapil M et al (2012) Hypoxic conditions induce a Cancer-like phenotype in human breast epithelial cells. PLoS One 7:e46543

Venugopalan G et al (2014) Multicellular architecture of malignant breast epithelia influences mechanics. PLoS One 9:e101955

Vidi P, Bissell MJ, Lelièvre SA (2013) Epithelial Cell Culture Protocols 945:193–219

Vinci M et al (2012) Advances in establishment and analysis of three-dimensional tumor spheroid-based functional assays for target validation and drug evaluation. BMC Biol 10:29

Wang M et al (2017) Role of tumor microenvironment in tumorigenesis. J Cancer 8:761–773

Weeber F, Ooft SN, Dijkstra KK, Voest EE (2017) Tumor organoids as a pre-clinical Cancer model for drug discovery. Cell Chem Biol 24: 1092–1100

Wellings SR (1980) A hypothesis of the origin of human breast cancer from the terminal ductal lobular unit. Pathol Res Pract 166:515–535

Wetering M, De V et al (2015) Prospective derivation of a living organoid biobank of colorectal Cancer patients resource prospective derivation of a living organoid biobank of colorectal Cancer patients. Cell 161:933–945

Wu D, Yotnda P (2011) Induction and testing of hypoxia in cell culture. J Vis Exp:4–7. https://doi.org/10.3791/2899

Yin X et al (2016) Cell stem cell engineering stem cell organoids. Stem Cell 18:25–38

Zanoni M et al (2016) 3D tumor spheroid models for in vitro therapeutic screening: a systematic approach to enhance the biological relevance of data obtained. Sci Rep 6:1–11

Zhang J et al (2015) TGF- b – induced epithelial-to-mesenchymal transition proceeds through stepwise activation of multiple feedback loops. Sci Signal 7:1–12

Zhou Y et al (2013) Multiparameter analyses of three-dimensionally cultured tumor spheroids based on respiratory activity and comprehensive gene expression profiles. Anal Biochem 439:187–193

Zhu J, Xiong G, Trinkle C (2014) Xu, R. integrated extracellular matrix signaling in mammary gland development and breast cancer progression. Histol Histopathol 29:1083–1092

Ziółkowska K et al (2012) Development of a three-dimensional microfluidic system for long-term tumor spheroid culture. Sensors Actuators B Chem 173:908–913